ACS APPLIED MATERIALS & INTERFACES

Open Access
This article is licensed under CC-BY-NC-ND 4.0

www.acsami.org
Research Article

MoS_2/Mayenite Electride Hybrid as a Cathode Host for Suppressing Polysulfide Shuttling and Promoting Kinetics in Lithium−Sulfur Batteries

Niphat Thatsami, Parinya Tangpakonsab, Pornsawan Sikam, Tanveer Hussain, Orapa Tamwattana, Anucha Watcharapasorn, Pairot Moontragoon, Biswarup Pathak, and Thanayut Kaewmaraya*

Cite This: ACS Appl. Mater. Interfaces 2024, 16, 37994−38005

Read Online

ACCESS | Metrics & More | Article Recommendations | Supporting Information

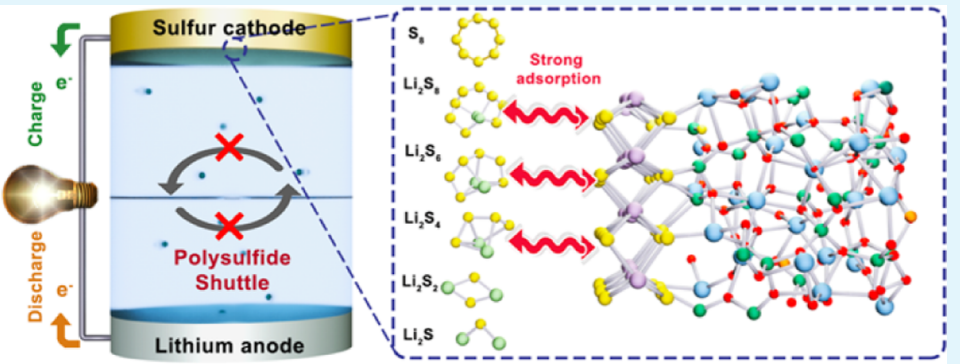

ABSTRACT: The commercial viability of emerging lithium−sulfur batteries (LSBs) remains greatly hindered by short lifespans caused by electrically insulating sulfur, lithium polysulfides (Li_2S_n; $1 \leq n \leq 8$) shuttling, and sluggish sulfur reduction reactions (SRRs). This work proposes the utilization of a hybrid composed of sulfiphilic MoS_2 and mayenite electride (C12A7:e^-) as a cathode host to address these challenges. Specifically, abundant cement-based C12A7:e^- is the most stable inorganic electride, possessing the ultimate electrical conductivity and low work function. Through density functional theory simulations, the key aspects of the MoS_2/C12A7:e^- hybrid including electronic properties, interfacial binding with Li_2S_n, Li^+ diffusion, and SRR have been unraveled. Our findings reveal the rational rules for MoS_2 as an efficient cathode host by enhancing its mutual electrical conductivity and surface polarity *via* MoS_2/C12A7:e^-. The improved electrical conductivity of MoS_2 is attributed to the electron donation from C12A7:e^- to MoS_2, yielding a semiconductor-to-metal transition. The resultant band positions of MoS_2/C12A7:e^- are well matched with those of conventional current-collecting materials (*i.e.*, Cu and Ni), electrochemically enhancing the electronic transport. The accepted charge also intensifies MoS_2 surface polarity for attracting polar Li_2S_n by forming stronger bonds with Li_2S_n via ionic Li−S bonds than electrolytes with Li_2S_n, thereby preventing polysulfide shuttling. Importantly, MoS_2/C12A7:e^- not only promotes rapid reaction kinetics by reducing ionic diffusion barriers but also lowers the Gibbs free energies of the SRR for effective S_8-to-Li_2S conversion. Beyond the reported applications of C12A7:e^-, this work highlights its functionality as an electrode material to boost the efficiency of LSBs.

KEYWORDS: *Li−S batteries, polysulfide shuttling, C12A7 electride, density functional theory, sulfur reduction reaction*

Downloaded via UNIV OF NEW ENGLAND on November 6, 2024 at 05:13:53 (UTC).
See https://pubs.acs.org/sharingguidelines for options on how to legitimately share published articles.

INTRODUCTION

Lithium-ion batteries (LIBs) are currently the mainstream storage devices for portable electronic gadgets and electric vehicles (EVs).[1] Nevertheless, the limited theoretical capacity (<387 Wh kg^{-1}) of LIBs elusively suffices overwhelming demands for ultrahigh energy densities toward extended-range EVs, smart grid applications, and ambitious electric aviation.[2,3] In this regard, rechargeable lithium−sulfur batteries (LSBs) have emerged as promising alternatives because of their ultimate theoretical energy density of 2600 Wh kg^{-1}, around five times greater than LIBs.[4] Moreover, the use of sulfur (i.e., the 10th most earth-abundant element) as an electrode material not only enhances sustainability due to its abundance but also leverages its status as a byproduct of the petroleum industry.[1] These technical advantages position LSBs as leading contenders among next-generation battery technologies.[5]

Received: April 12, 2024
Revised: July 3, 2024
Accepted: July 3, 2024
Published: July 10, 2024

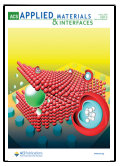

© 2024 American Chemical Society

https://doi.org/10.1021/acsami.4c05810
ACS Appl. Mater. Interfaces 2024, 16, 37994−38005

Despite their numerous benefits, the technological readiness level of LSBs is around 7−8, meaning full commercialization is not available at the moment.[6] LSBs typically face manifold challenges associated with the intrinsic properties of the cathode, electrolyte, and anode.[5,7] The sulfur cathode is both electronic ($\sigma_e = 5 \times 10^{-15}$ S m^{-1}) and ionic insulator, which retards electrochemical kinetics.[8] The conversion of elemental sulfur (S_8) into end-product lithium sulfide (Li_2S) during the sulfur reduction reaction (SRR) involves the subtle 16-electron process (*i.e.*, $S_8 + 16Li^+ + 16e^- = 8Li_2S$), yielding various heteropolar lithium polysulfides (Li_2S_n; $1 \leq n \leq 8$).[9] In particular, the transitions among Li_2S_n are energetically hindered by the sluggish SRR derived from the solid−liquid−solid phase evolution. Additionally, certain high-order polysulfides (Li_2S_n; $4 \leq n \leq 8$) can be readily dissolved in polar liquid electrolytes, such as common 1,2-dimethoxyethane (DME) and 1,3-dioxolane (DOL).[10] This intricate solubility phenomenon, known as polysulfide shuttling, gradually depletes the active polysulfides, which are subsequently migrated backward to deposit as dendrites at the anode. Consequently, an electrically insulating solid−electrolyte interface is formed at the anode.[10] Thus, the battery's capacity retention and Coulombic efficiency are severely suppressed.[11] Furthermore, the end-product Li_2S of SRR induces substantial volumetric expansion of around 80.0% because of the pronounced difference in volumetric densities between S_8 and Li_2S.[5] This results in cathode mechanical instability and shortened battery lifespan.[5] Addressing these challenges is essential for enhancing the performance of LSBs.

One feasible route to overcoming these technical challenges is through the strategic utilization of the cathode hosting material, also known as the cathode anchoring material.[12] The host should possess certain desirable features including high electrical conductivity, a sulfiphilic surface, rich surface area, and superior mechanical flexibility.[12] High electrical conductivity is essential for efficient electrochemical reactions.[5] The sulfiphilic characteristics facilitate the anchoring of mobile redox centers to directly use chemically adsorbed polysulfides, which bind to the host stronger than polysulfides with electrolytes (*i.e.*, inhibiting the polysulfide solubility). This accelerates Li_2S chemical kinetics and homogeneous growth.[13] The ultrahigh surface area maximizes polysulfide chemisorption possibilities, thereby improving sulfur utilization.[13] Furthermore, exceptional mechanical flexibility is crucial for tolerating cathode volumetric expansion/contraction during lithiation/delithiation.[5] Given these requirements, generic two-dimensional (2D) materials become the promising candidates due to their high electrical conductivity, planar geometry with enriched surface area and chemistry, and superior mechanical flexibility.[14] Accordingly, numerous works have reported the successful implementations of 2D hosting materials for enhancing the efficiencies of LSBs such as graphene,[15] S-terminated Ti_2C MXenes,[16] biphenylene,[17] carbon nitrides C_xN_y,[18] germanene,[19] antimonene,[20] and generic transition metal dichalcogenides (TMDs).[21] Their major accomplishments can be attributed to their sulfiphilic nature for effectively inhibiting polysulfide shuttling and their electrocatalytic properties for accelerating electrochemical reactions.

Among various 2D materials, molybdenum disulfide (MoS_2), a reputed 2D material in the family of TMDs, has received intensive attention as the cathode host for LSBs owing to its natural abundance, sulfiphilic nature, ultrafast carrier mobility, less surface dangling bonds with minimal charge trapping, superior mechanical flexibility, and doping engineering and functionalization of 2D metal chalcogenides.[22] Importantly, MoS_2 can be mass-produced *via* liquid exfoliation and chemical vapor deposition techniques.[23] Nevertheless, the obtained battery performance of LSBs based on MoS_2 mandates further improvements (*i.e.*, unfavorable rate performance and poor cycling durability) because of inadequate electrical conductivity and sluggish reaction kinetics during cycling.[24] The electronic conductivity and redox kinetics of MoS_2 can be exemplarily improved by employing sulfur-doped graphene frameworks supporting atomically dispersed 2H−MoS_2,[25] sodiated MoS_2,[26] and MoS_2/MoN lateral heterostructures.[27] In particular, the enhanced performance in the MoS_2/MoN heterostructure is attributed to the electron donation from MoN to MoS_2. As a result, MoS_2 is n-doped and becomes more electrically conductive to accelerate the redox reaction of polysulfides and smoothen Li^+ diffusion pathways.[26] Moreover, the concept of heterostructures for magnifying conductivity extends to van der Waals heterostructures (vdWHs)[28] in which distinct 2D materials are vertically assembled *via* vdW interaction. Specifically, vdWHs comprising $MoTe_2$ and 2D electride $[Ca_2N]^+$:e^- enable ultimate electronic transport of $MoTe_2$ (*i.e.*, carrier concentration of 1.6×10^{14} cm^{-2} and a prolonged electron diffusion length of around 100 nm).[28] Inspired by these previous works, it is postulated that one can enhance battery performance by rationally utilizing a hybrid cathode host made from sulfiphilic MoS_2. This host is coupled with a highly electrically conductive, electron-rich, chemically and thermally stable, low work function, and naturally abundant electron-donor material.

Given the requirements mentioned above, novel electride materials are potential candidates. The electride phase defines peculiar ionic compounds consisting of positively and negatively charged ions.[29] The negative ions are simply electrons without nuclei which are weakly bound in the host structure, thereby acting as an electron gas to render superlative electron transport and a platform for topological materials.[29] In 2003, the earth-abundant mineral mayenite ($[Ca_{12}Al_{14}O_{33}]^{4+}$:$4O^{2-}$ or simply known as C12A7), a compound in the family of cement-based calcium aluminates, was synthesized as the electride variant by extracting O^{2-} ions from the C12A7 structure *via* chemical reduction and replacing them by anionic electrons.[30] The resultant chemical formula is $[Ca_{12}Al_{14}O_{33}]^{4+}$:$4e^-$ abbreviated to C12A7:e^-. Unlike air-susceptible 2D electride $[Ca_2N]^+$:e^-, C12A7:e^- is intriguingly the first inorganic electride thermally and chemically stable at ambient conditions.[31] C12A7:e^- exhibits exceptional electrical mobility and transport (conductivity reaching 1500 S cm^{-1} at room temperature), excellent electron concentration (2.0×10^{23} cm^{-3}), ultralow work function (around 2.4 eV),[31] and exceptional mechanical flexibility.[32] The unique features enable numerous applications including superconductivity (the critical temperature 0.2−0.4 K), electron-field emitters,[33] display devices, catalysis for ambient pressure ammonia production,[34] and transparent conductive oxides.[35] Beyond these, C12A7:e^- is a promising material serving as an appropriate electron donor to intensify the electron transport and catalytic surface reactivity of MoS_2 when combined as a heterostructure. In other words, the MoS_2/C12A7:e^- hybrid is hypothesized to be an efficient conductive host for circumventing the insulating nature of sulfur, inhibiting the shuttle effect, and enhancing the electrochemical reactions in LSBs.

Herein, this work aims at using the MoS_2/mayenite electride (C12A7:e^-) hybrid as the cathode host to resolve limitations of

https://doi.org/10.1021/acsami.4c05810
ACS Appl. Mater. Interfaces 2024, 16, 37994−38005

LSBs. Density functional theory (DFT) was employed to unravel the key aspects including electronic properties, the interfacial binding of Li_2S_n on MoS_2/C12A7:e^-, Li^+ diffusion, charge transfer mechanism, and SRR. We discovered that the MoS_2/mayenite electride hybrid as a cathode host can effectively suppress polysulfide shuttling while enhancing reaction kinetics in LSBs. Apart from the known applications of C12A7:e^-, this work sheds light on its unique role as an electrode material in LSBs.

MODELING AND COMPUTATIONAL DETAILS

MoS_2/C12A7:e^- was considered as a hosting material for the sulfur cathode. Modeling of the MoS_2/C12A7:e^- atomic structure was based on the optimized 4 × 4 × 1 supercell of the single-layer MoS_2 unit cell ($a = b = 3.18$ Å, c = 15.00 Å) placed on top of the cubic unit cell of C12A7:e^-, resulting in a 166-atom unit cell. The C12A7:e^-(100) plane was considered because it was successfully fabricated in the experiment.[36] An adequate 15.0 Å vacuum gap was incorporated in the vertical direction of the pristine MoS_2 and MoS_2/C12A7:e^- hybrids to eliminate self-interactions among periodic replicas.

DFT *via* the Vienna Ab initio Simulation Package (VASP)[37,38] was employed to unravel the fundamental aspects of LSBs. The gradient-corrected Perdew−Burke−Ernzerhof (PBE) formalism was adopted to describe the exchange−correlation energy.[39] The projector augmented wave was used to circumvent the rapidly oscillating wave functions of electrons near the ion cores.[40] Here, the Mo ($4p^6\ 5s^1\ 4d^5$), S ($3s^2\ 3p^4$), Ca ($3s^2\ 3p^6\ 4s^2$), Al ($3s^2\ 3p^1$), O ($2s^2\ 2p^4$), and Li ($1s^2\ 2s^1$) were treated as the valence states in our calculations. Based on the modeled atomic structures, we employed the converged energy cutoff of 600.0 eV with the Brillouin zone integration of 3 × 3 × 1 (9 × 9 × 1) Monkhorst−Pack grids for structural optimization (calculation of electronic density of states).[41] The structural optimization relied on the convergence criterion of Hellmann−Feynman forces acting on each atom (*i.e.*, 20.0 meV/Å.). The total energies of the modeled structures were iteratively minimized until the energy difference between the two consecutive cycles of electronic self-consistency was less than 10^{-6} eV. Spin−orbit coupling was not considered in our work.

Interfacial interactions of Li_2S_n on MoS_2 and MoS_2/C12A7:e^- were investigated by evaluating the binding energies (E_b) according to the following equation

$$E_b = E[MoS_2/C12A7{:}\ e^- + Li_2S_n] - E[MoS_2/C12A7{:}\ e^-] - E[Li_2S_n] \quad (1)$$

where the first, second, and third terms on the right-hand side of eq 1 define the total energies of Li_2S_n-adsorbed MoS_2/C12A7:e^-, bare MoS_2/C12A7:e^-, and isolated Li_2S_n, respectively. Intrinsic van der Waals (vdW) forces existing at the interface of Li_2S_n−MoS_2/C12A7:e^- were considered according to Grimme's DFT-D3 approach.[42] Furthermore, we calculated the ionic diffusion of Li^+ ions on pristine MoS_2 and MoS_2/C12A7:e^- using the climbing-image nudged elastic band (CI-NEB) method.[43] Insightful analysis of bonds formed between Li_2S_n and MoS_2/C12A7:e^- was carried out using the crystal orbital Hamilton population (COHP) which applies to studying chemical bonding in absorption, surface processes, and extended solids (*i.e.*, covalent, ionic, and metallic crystals).[44] COHP allocates the band-structure energy (here, DOS outputs from plane-wave-based VASP) to orbital−pair interactions (*i.e.*, bond-weighted DOS of a pair of nearby atoms). A COHP diagram indicates bonding and antibonding contributions to the band-structure energy. Moreover, the integrated COHP (ICOHP) represents the contribution of a certain bond to the band energy, hinting at the bond strength. Moreover, Bader charge analysis was conducted to quantify the net atomic charges based on the reconstructed (all-electron) valence density.[45]

Moreover, electrochemical reactions in LSBs were investigated through SRR which is of considerable interest for achieving high-density kinetics energy storage.[46] SRR defines a subtle 16-electron process for reversibly converting sulfur S_8 to the end-product Li_2S. Mathematically, the overall reaction can be written as $S_8 + 16Li^+ + 16e^- = 8Li_2S$ in which there are a series of intermediates Li_2S_n as follows[9]

$$^*S_8 + 2Li^+ + 2e^- = {}^*Li_2S_8 \quad (2)$$

$$^*Li_2S_8 = {}^*Li_2S_6 + 1/4S_8 \quad (3)$$

$$^*Li_2S_6 = {}^*Li_2S_4 + 1/4S_8 \quad (4)$$

$$^*Li_2S_4 = {}^*Li_2S_2 + 1/4S_8 \quad (5)$$

$$^*Li_2S_2 = {}^*Li_2S + 1/8S_8 \quad (6)$$

where * represents Li_2S_n which is bound on MoS_2 and MoS_2/C12A7:e^-. The changes in Gibbs free energy (ΔG) at constant pressure and temperature were calculated to quantify the feasibility of chemical reactions according to the equation $\Delta G = \Delta E + \Delta E_{ZPE} - T\Delta S$. Here, ΔE, ΔE_{ZPE}, and $T\Delta S$ denote the difference in the binding energies of Li_2S_n adsorbed on the host's surface, zero-point energy (ZPE) associated with molecular vibrations of Li_2S_n, and entropy variation between the Li_2S_n-adsorbed MoS_2 or MoS_2/C12A7:e^- and isolated Li_2S_n. All of the ΔG corresponding to the reaction stages (eqs 2−6) were computed as the following expressions

$$\Delta G_1 = [E_{*Li_2S_8} + E_{ZPE(*Li_2S_8)} - TS_{*(Li_2S_8)}] + [E_{*S_8} + E_{ZPE(*S_8)} - TS_{*(S_8)}] - 2[E_{Li} + E_{ZPT(Li)} - TS_{Li}] \quad (7)$$

$$\Delta G_2 = [E_{*Li_2S_6} + E_{ZPE(*Li_2S_6)} - TS_{*(Li_2S_6)}] + (1/4)[E_{*S_8} + E_{ZPE(*S_8)} - TS_{*(S_8)}] - [E_{*Li_2S_8} + E_{ZPE(*Li_2S_8)} - TS_{*(Li_2S_8)}] \quad (8)$$

$$\Delta G_3 = [E_{*Li_2S_4} + E_{ZPE(*Li_2S_4)} - TS_{*(Li_2S_4)}] + (1/4)[E_{*S_8} + E_{ZPE(*S_8)} - TS_{*(S_8)}] - [E_{*Li_2S_6} + E_{ZPE(*Li_2S_6)} - TS_{*(Li_2S_6)}] \quad (9)$$

$$\Delta G_4 = [E_{*Li_2S_2} + E_{ZPE(*Li_2S_2)} - TS_{*(Li_2S_2)}] + (1/4)[E_{*S_8} + E_{ZPE(*S_8)} - TS_{*(S_8)}] - [E_{*Li_2S_4} + E_{ZPE(*Li_2S_4)} - TS_{*(Li_2S_4)}] \quad (10)$$

$$\Delta G_5 = [E_{*Li_2S} + E_{ZPE(*Li_2S)} - TS_{*(Li_2S)}] + (1/8)[E_{*S_8} + E_{ZPE(*S_8)} - TS_{*(S_8)}] - [E_{*Li_2S_2} + E_{ZPE(*Li_2S_2)} - TS_{*(Li_2S_2)}] \quad (11)$$

https://doi.org/10.1021/acsami.4c05810
ACS Appl. Mater. Interfaces 2024, 16, 37994−38005

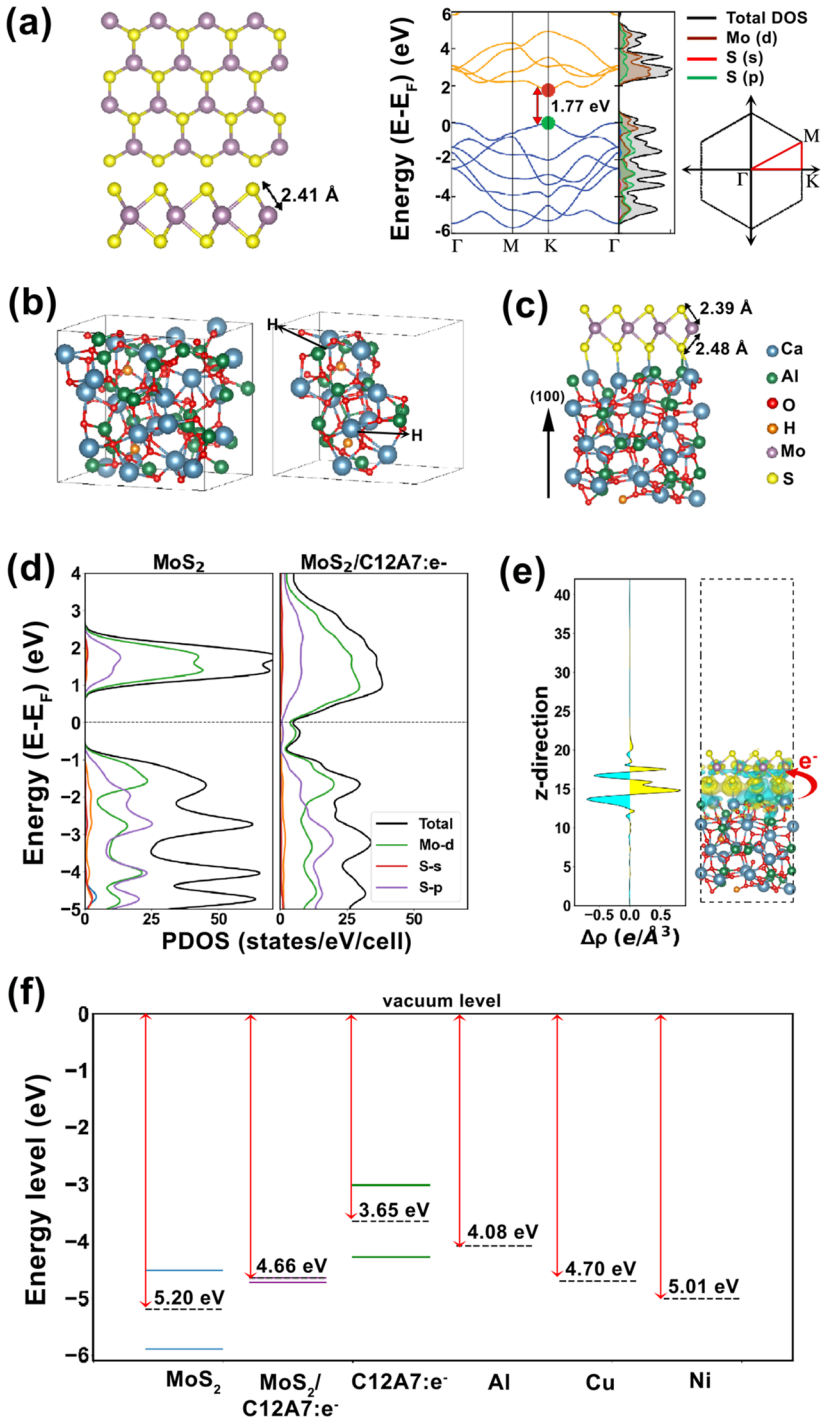

Figure 1. (a) Top and side view of the crystal structure, electronic band structure, and PDOS of MoS_2. (b,c) Optimized heterostructures of C12A7:e^- and MoS_2/C12A7:e^-. (d) PDOS of MoS_2 and optimized heterostructures of MoS_2/C12A7:e^-. (e) Charge density difference ($\Delta\rho$) between MoS_2 and MoS_2/C12A7:e^- as calculated by $\Delta\rho(\vec{r}) = \rho_{MoS_2/C12A7:e^-}(\vec{r}) - \rho_{C12A7:e^-}(\vec{r}) - \rho_{MoS_2}(\vec{r})$. The isosurface is set to be 0.001 e/Å^3. (f) Band alignment diagram of MoS_2, C12A7:e^-, MoS_2/C12A7:e^- hybrid, and conventional current collectors (*e.g.*, Al, Cu, and Ni).

We set the temperature to ambient 298.15 K. ZPE was obtained by performing vibrational frequency calculations of Li_2S_n on MoS_2 and MoS_2/C12A7:e^- by calculating the second-order derivatives of the total energy with respect to the ionic positions *via* a method of finite differences. The atomic positions of MoS_2 and MoS_2/C12A7:e^- were fixed during the calculations, whereas those of Li_2S_n were allowed to move. Furthermore, the ΔG energies for the SRR of Li_2S_n in a vacuum are also comparatively calculated to justify the role of the cathode hosts in the SRR.

RESULTS AND DISCUSSION

Structural Properties of MoS_2 and C12A7:e^- Electride.

As the first step, Figure 1a shows the crystal structure of monolayer MoS_2. It is classified as a threefold-hexagonal symmetry with the space group $P\bar{6}m2$ (no. 187).[47] The S−Mo−S sandwich structure possesses the optimized lattice

https://doi.org/10.1021/acsami.4c05810
ACS Appl. Mater. Interfaces 2024, 16, 37994−38005

constant of a = 3.18 Å, and the Mo−S and S−S bond lengths are 2.41 and 3.11 Å, respectively. These crystallographic parameters are consistent with the reported works.[48] Moreover, the electronic projected density of states (PDOSs) and the corresponding band structure as calculated by the PBE level of theory manifest a finite direct bandgap of 1.77 eV, agreeing with the reported value of 1.80 eV.[49] Meanwhile, Figure 1b shows an optimized unit cell of the C12A7:e^- electride comprising empty and occupied cages. There are two oppositely charged components including (i) positive $[Ca_{24}Al_{28}O_{64}]^{4+}$ and (ii) negative $(H^-)_2$. The first part represents a positively charged framework consisting of 12 crystallographic cages. The second part denotes a negatively charged extra-framework that occupies the 2 off-center cages. All cages exhibit S_4 symmetry, where the symmetry axes pass through the cage poles (Ca−Ca). The calculated lattice constant a is 12.09 Å, respectively. The average Ca−Ca distance along the cage poles in empty cages is 5.73 Å, whereas that in the cages occupied by electrons is 4.18 Å. The electronic density of states and band structure of C12A7:e^- are shown in Figure S1.[50]

Subsequently, Figure 1c depicts the relaxed atomic geometry of the MoS_2/C12A7:e^- heterostructure. MoS_2 in the hybrid shows slight deformation as evidenced by the infinitesimal 0.83% deviation in the Mo−S bond lengths (2.39 and 2.48 Å as compared with original 2.41 Å in pristine MoS_2). Likewise, the crystal structure of C12A7:e^- in the heterostructure remains virtually retained as compared to the original C12A7:e^- because there are small expansions in Ca−O and Al−O distances at the interface. Quantitatively, the Ca−O and Al−O distances at the surface before (after) making the heterostructure are 2.28 Å (2.34) Å and 1.82 Å (1.84 Å), amounting to 6.0 and 1.0% enlargements, respectively. Hence, both MoS_2 and C12A7:e^- nearly conserved their structural features after being merged into the heterostructure. This implies that the fabricated MoS_2/C12A7:e^- sample exhibits X-ray diffraction patterns of the component materials resembling their bulk counterparts. Intriguingly, there are bridging S−Ca bonds with the average bond distance of 2.48 Å formed at the boundary. This length is close to the sum of the ionic radii of Ca (1.84 Å) and S (1.00 Å) atoms[51] and 2.549 Å of an ionic Ca−S bond in rock-salt CaS,[52] indicating that the interface is dominated by ionic chemisorption.

Figure 1d comparatively shows the PDOS of MoS_2 before and after being combined with C12A7:e^-. MoS_2 in the MoS_2/C12A7:e^- heterostructure adopts the metallic state characterized by the finite states of S-3p and Mo-4d orbitals at the Fermi energy. The resultant metallic character of MoS_2 as an electrode material is beneficial for enhancing the electrochemical process in LSBs.[5] Such semiconductor-to-metal transition is attributed to the formation of ionic S−Ca bonds at the boundary because the S atoms are highly more electronegative than the Ca atoms.[53] This results in notable charge transfer from C12A7:e^- to MoS_2 as evidenced by the charge density difference plot in Figure 1e. Quantitatively, Bader charge analysis further indicates that Mo and interfacial S atoms accept 0.12e^- from C12A7:e^-, yielding the modification of Mo−S bond distances. Furthermore, the charge transfer mechanism is also contributed by the electron flow from C12A7:e^- to MoS_2 because of the lower work function of the former as depicted in Figure 1f. The accepted charges in MoS_2 help intensify the surface chemical reactivity for interacting with heteropolar Li_2S_n. The work function of MoS_2/C12A7:e^- is calculated to be 4.65 eV which is well matched with those of current-collecting materials of battery devices such as Cu (4.70 eV) and Ni (5.01 eV).[54] The metallic feature of MoS_2 and the appropriate work function of MoS_2/C12A7:e^- consequently facilitate electronic transport for accelerating the electrochemical process in LSBs.

Binding characteristics of Li_2S_n with MoS_2 and MoS_2/C12A7:e^-

It is expected that charge donation from C12A7:e^- to MoS_2 enhances MoS_2/C12A7:e^- surface affinity toward heteropolar Li_2S_n.[13] Pristine MoS_2 and MoS_2/C12A7:e^- heterostructure are then utilized as the cathode host material to anchor Li_2S_n binding.[55] Li_2S_n-DME/DOL binding is also considered as a reference for justifying polysulfide shuttling suppression. The lowest-energy conformation of each Li_2S_n adsorbed on MoS_2 and MoS_2/C12A7:e^- is obtained by attempting various adsorption orientations and sites. Figure 2 exclusively assembles the lowest-energy atomic configurations of Li_2S_n adsorbed on

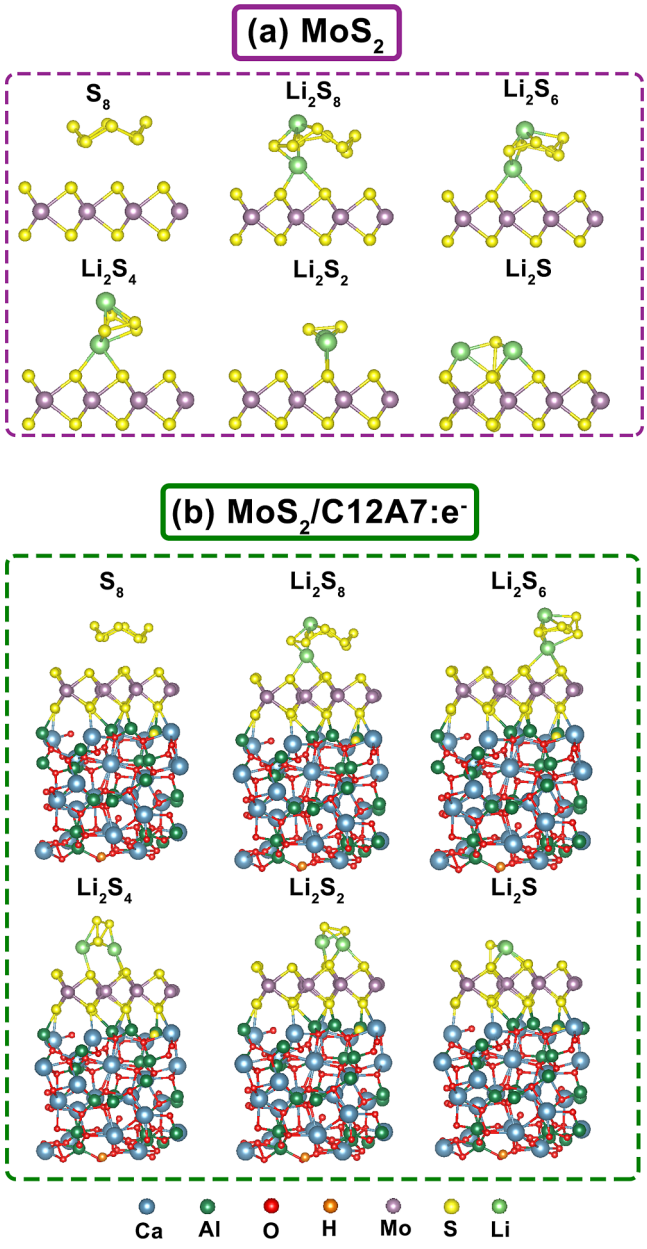

Figure 2. Optimized structures of Li_2S_n adsorbed on (a) MoS_2 and (b) MoS_2/C12A7:e^-.

https://doi.org/10.1021/acsami.4c05810
ACS Appl. Mater. Interfaces 2024, 16, 37994−38005

MoS_2 and MoS_2/C12A7:e^-. One can see that S_8 energetically adopted the parallel orientation on both MoS_2 and MoS_2/C12A7:e^- for intensifying the interfacial interaction, resembling the horizontal adsorption configuration observed in 2D anchoring materials such as graphene,[55] black phosphorene,[56] Fe_3C,[57] and MXenes.[16] The bond distances from S_8 to MoS_2 (MoS_2/C12A7:e^-) are 3.37 (3.27) Å which are twice the atomic radius of S (1.00 Å).[51] Hence, S_8 is physisorbed on MoS_2 (MoS_2/C12A7:e^-) *via* predominant vdW forces. Notably, the relatively shorter S_8−MoS_2/C12A7:e^- distance manifests that S_8 on MoS_2/C12A7:e^- experiences enhanced interaction than that in pristine MoS_2.

Meanwhile, Li_2S_n is adsorbed on MoS_2 and MoS_2/C12A7:e^- by forming Li−S bonds. This scenario is likely driven by the drastic difference in the electronegativity values between S (2.58) and Li (0.98).[53] The energetically dissociative adsorption of all polysulfides on MoS_2 and MoS_2/C12A7:e^- is not observed, ensuring Li_2S_n conversion reversibility in the redox reaction. Li_2S_n−MoS_2 bond distances range from 2.20 to 2.58 Å. These distances are within the combination of atomic radii of S (1.00 Å) and Li (1.45 Å),[51] characterizing the chemical S−Li bonds formed at the boundary. Notably, the MoS_2/C12A7:e^- composite induces a stronger interaction with Li_2S_n. The shortened bond distances of Li_2S_n−MoS_2/C12A7:e^- range from 2.08 to 2.58 Å. In addition, we calculated the binding energies associated with the structural conformations presented by using eq 1. All obtained binding energies are negative, indicating the attractive interaction. However, Figure 3 shows

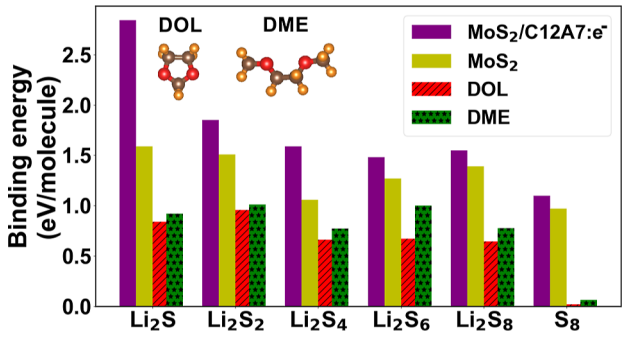

Figure 3. Magnitudes of binding energies of Li_2S_n adsorbed on MoS_2 and MoS_2/C12A7:e-. Here, DOL and DME abbreviate 1,3-dioxolane and 1,2-dimethoxyethane, respectively, which are common electrolytes used in LSBs.

the strengths of the binding energies (E_b) of S_8 and Li_2S_n on MoS_2 and MoS_2/C12A7:e^-. There are significant differences in the adsorption energies of Li_2S_4, Li_2S_2, and Li_2S adsorbed on pristine MoS_2 compared to their adsorption on MoS_2/C12A7:e^-. This is due to the markedly different geometrical orientations of Li_2S_4, Li_2S_2, and Li_2S adsorbed on pristine MoS_2 vs those on MoS_2/C12A7:e^-. In contrast, Li_2S_6, Li_2S_8, and S_8 exhibit virtually similar orientations on both MoS_2 and MoS_2/C12A7:e^-, resulting in less pronounced differences in the adsorption energies. The Li_2S_n is adsorbed on MoS_2 with competitively stronger E_b than DME and DOL, in accordance with reported works.[58] Besides, the MoS_2/C12A7:e^- heterostructure further strengthens the interactions with polysulfide species compared with pristine MoS_2. The E_b values of Li_2S_n on MoS_2/C12A7:e^- surpass those on DME and DOL. In particular, MoS_2/C12A7:e^- greatly maximizes the binding of the liquid high and medium S-content polysulfides (Li_2S_n, where n = 8, 6, and 4) which are the liquid phases and highly susceptible to dissolution (*i.e.*, the major cause of polysulfide shuttling).[9] Hence, it is conclusive that MoS_2/C12A7:e^- as the cathode host effectively suppresses polysulfide shuttling.

Electronic Properties of MoS_2/C12A7:e^- Interacting with Li_2S_n. The strong binding affinities between Li_2S_n and MoS_2/C12A7:e^- are responsible for the suppression of polysulfide shuttling. Moreover, analyzing the variations in the electronic properties of Li_2S_n when interacting with MoS_2/C12A7:e^- is crucial for comprehending the chemical bonds formed between Li_2S_n and MoS_2/C12A7:e^-. Figure 4a−f displays the total density of states (TDOSs) of Li_2S_n before and after adsorption. The bulk sulfur (cyclo-S_8) is categorized as an insulator because of its large finite energy gap. Notably, the TDOS of S_8 undergoes a notable change after adsorption. Likewise, all Li_2S_n intermediates are characterized as electrical insulators owing to the finite energy gaps. Their TDOSs undergo remarkable variations after interacting with MoS_2/C12A7:e^-, attesting to chemisorption. Furthermore, we calculated charge density difference ($\Delta\rho$) to support TDOS analysis according to the following expression

$$\Delta\rho = \rho[MoS_2/C12A7{:}\ e^- + Li_2S_n] - \rho[MoS_2/C12A7{:}\ e^-] - \rho[Li_2S_n] \quad (12)$$

where the first, second, and third terms on the right-hand side of eq 12 represent the electron density of the Li_2S_n-adsorbed MoS_2/C12A7:e^-, MoS_2/C12A7:e^-, and the corresponding isolated Li_2S_n molecule, respectively. Figure 4c,d illustrates $\Delta\rho$ of the polysulfides adsorbed on MoS_2/C12A7:e^-. The adsorption of bulk S_8 on MoS_2/C12A7:e^- causes insignificant charge redistribution, consistent with the weak E_b values and indicative of predominant physisorption. By contrast, the charge transfer becomes pronounced in the case of Li_2S_6, supporting enhanced E_b values and a tendency toward predominant chemisorption. Specifically, Li_2S_6 donates charges to the MoS_2/C12A7:e^- host, resulting in an upshift in the TDOS of the host, as described previously. Likewise, charge transfer is particularly immense in Li_2S, supporting the notion of prominent chemisorption.

Additionally, the amount of charge transfer is computed using the Bader charge approach, as shown in Figure 5a. Quantitatively, S_8, Li_2S_6, and Li_2S donate 0.0004e (0.0005e), 0.003e (0.006e), and 0.02e (0.03e) to MoS_2 (MoS_2/C12A7:e^-), respectively. The donated charges consequently magnify the Li_2S_n−MoS_2/C12A7:e^- interactions as shown by the analysis of PDOS and COHP in Figure 5b−d. The S-3p orbitals from S_8 weakly interact with those from MoS_2/C12A7:e^-, resulting in infinitesimal ICOHP of −0.097 eV/bond. By contrast, there are immense chemical interplays among Li-2s of Li_2S_n (here, selectively shown by high S-content Li_2S_6 and low S-content Li_2S), S-3s, and S-3p orbitals of MoS_2/C12A7:e^-, as indicated by the antibonding peaks in the conduction band. These antibonding peaks are derived from the charge donation from the Li-2s state to S-3s and S-3p states to form antibonding states of ionic Li−S bonds above the Fermi energy. Moreover, these bonds possess pronounced bond energies, as indicated by the maximized ICOHP of −0.539 and −0.767 eV/bond for Li_2S_6 and Li_2S, respectively. Note that the shape of the Mo-4d states remains nearly conserved during the interaction with Li_2S_n. This is because the atomic geometry of MoS_2 comprises the Mo atoms in the central sublayer sandwiched by the outer S atoms. Thus, they do not directly interact with Li_2S_n.[59] Based on our

https://doi.org/10.1021/acsami.4c05810
ACS Appl. Mater. Interfaces 2024, 16, 37994−38005

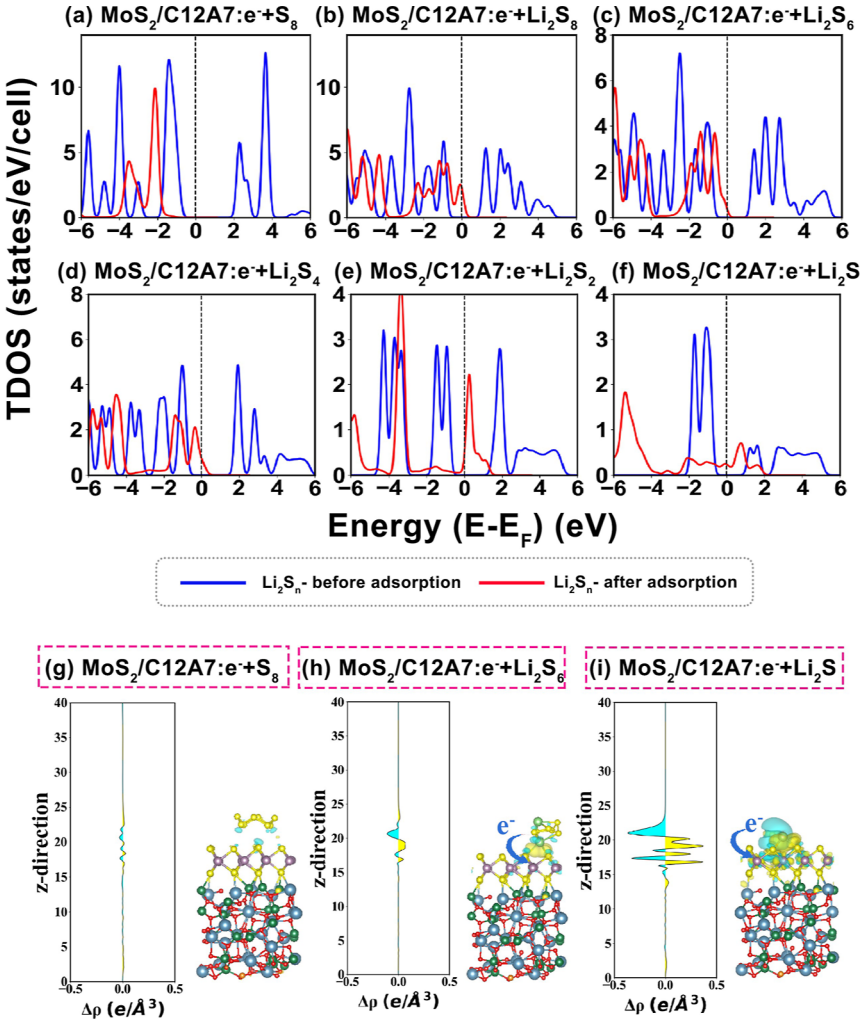

Figure 4. (a–f) TDOS of Li_2S_n before and after interacting with MoS_2/C12A7:e^-. The Fermi energy is shifted to zero for the sake of comparative visualization. (g,i) Charge density difference between Li_2S_n-adsorbed MoS_2/C12A7:e^-.

analysis of electronic properties, charge-transfer ionic Li–S bonds formed at the Li_2S_n–MoS_2/C12A7:e^- interface are conclusively responsible for mitigating polysulfide dissolution in DOL and DME electrolytes.

Li^+ Ionic Diffusion. Li^+ ionic diffusivity on the cathode of LSBs plays a central role in the reaction kinetics of polysulfide conversion in the redox reaction process as probed by an electrochemical current–voltage measurement.[60] The Li^+ ions energetically favor the low diffusion energy to maximize the diffusion rate basically according to Arrhenius equation $k = Ae^{-E_a/RT}$, where k, A, E_a, R, and T represent the rate constant, frequency factor depending on the lattice vibrations of diffusion state, diffusion barrier, universal gas constant, and temperature, respectively.[61] In particular, low diffusion energy at a finite temperature on the surface of anchoring materials can particularly enhance the chemical reaction between lithium (anode) and sulfur (cathode).[62] According to this, we compute the diffusion barriers of Li^+ ions on MoS_2 and MoS_2/C12A7:e^- using the CI-NEB approach to justify the catalytic anchoring roles of MoS_2 and MoS_2/C12A7:e^- in lowering the diffusion potentials. Figure 6a–c shows the diffusion profiles and most energetic paths of the Li^+ ion on MoS_2 and MoS_2/C12A7:e^-. The preferential route is obtained by considering the path connecting two neighboring points on the surfaces of MoS_2 and MoS_2/C12A7:e^- at which the E_b values of Li^+ are the strongest. The diffusion barriers of Li^+ on pristine MoS_2, interfacial-strained MoS_2, and MoS_2/C12A7:e^- are 0.25,[63] 0.15, and 0.12 eV, respectively. The interfacial-strained MoS_2 here defines the intrinsic strain imposed by the lattice mismatch between MoS_2 and C12A7:e^-. The reduction in the ionic diffusion barrier in MoS_2/C12A7:e^- is simultaneously contributed by (i) the interfacial strain imposing on MoS_2 from the lattice incompatibility and (ii) the charge transfer between MoS_2 and C12A7:e^-. Notably, the strain plays a more dominating role, accounting for more than 50% of the barrier reduction. The pathway follows a curved trajectory between the adjacent hollow sites of the Mo–S hexagons.[62] This is because the ion follows the path experiencing less potential, which is the hollow site above the inner Mo atoms. The presence of C12A7:e^- remarkably reduces the barrier, evidencing its catalytic ability for Li^+ ions' mobility when in contact with MoS_2. Moreover, the obtained values are among the lowest as compared to those of 2D materials such as graphene (0.32 eV),[64] single-atom-catalyzed graphene,[65] a family of metal sulfides (0.12–0.26 eV),[60] and Ti_2CS_2 MXenes (0.12 eV),[16] all calculated from the similar DFT-based NEB approach. The variations in the ionic potential profiles of MoS_2 and MoS_2/C12A7:e^- are associated with the metallic nature of MoS_2 in the MoS_2/C12A7:e^- hybrid as compared with the

https://doi.org/10.1021/acsami.4c05810
ACS Appl. Mater. Interfaces 2024, 16, 37994–38005

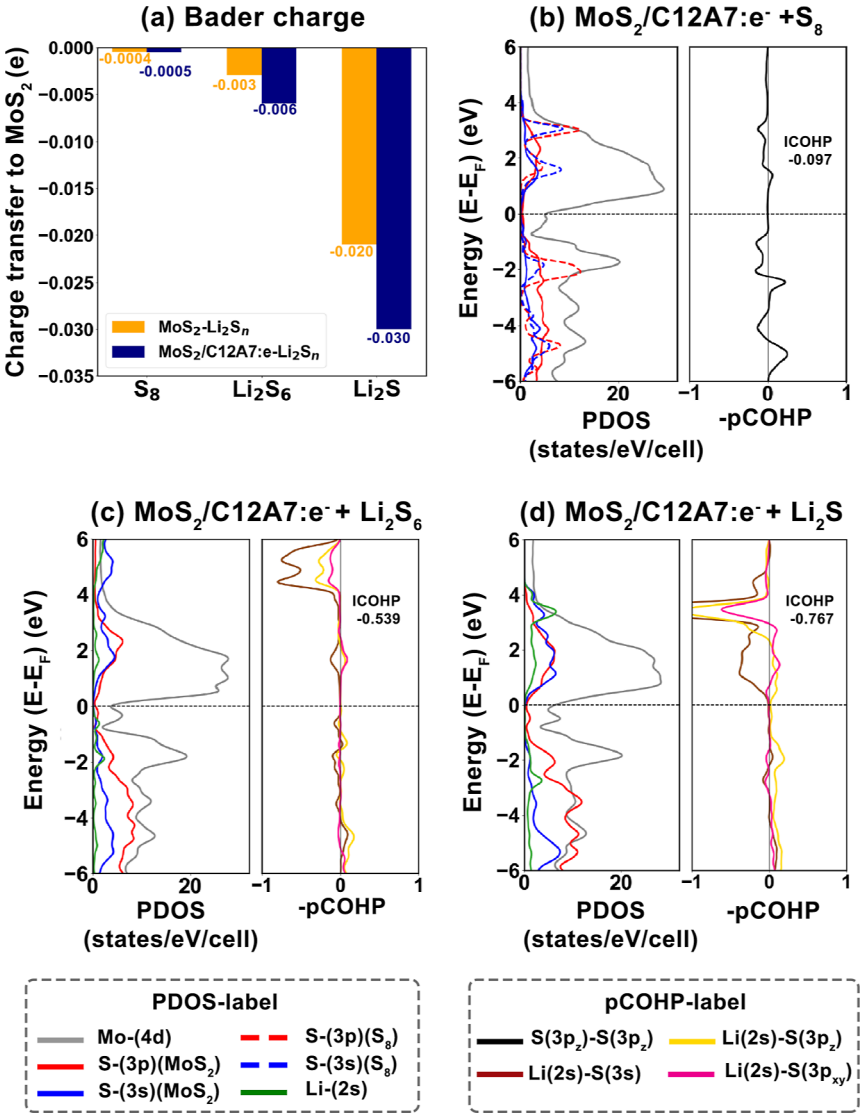

Figure 5. (a) Bar chart of Bader charge transfer from Li_2S_n to MoS_2 and MoS_2/C12A7:e^-. (b–d) PDOS of Li_2S_n-adsorbed MoS_2/C12A7:e^- in which the corresponding COHP and ICOHP of the bonds between Li (S) of Li_2S_n and MoS_2/C12A7:e^- are also shown.

original semiconducting MoS_2. According to the d-band model in metal catalysts,[66] the d-band center (ε_d) is quantitatively computed by the following expression

$$\varepsilon_d = \frac{\int_{-\infty}^{+\infty} n_d \varepsilon d\varepsilon}{\int_{-\infty}^{+\infty} n_d d\varepsilon} \quad (13)$$

where ε and n_d denote the energy and DOS of the Mo-3d states integrated in a particular range of energy. Moreover, the p-band centers are determined using the same concept as in eq 13.[9] The ε_d values of Mo-3d states in MoS_2 and MoS_2/C12A7:e^- are −3.08 and −3.03 eV, respectively. The values of Mo p-band centers in MoS_2 and MoS_2/C12A7:e^- are −3.335 and −3.554 eV, respectively. Meanwhile, those of S p-band centers in MoS_2 and MoS_2/C12A7:e^- are −3.463 and −3.722 eV, respectively. In particular, the upshift in the S-3p states intensifies the interaction with Li-s states, being consistent with the COHP bonding analysis and Bader charge analysis as presented in the former section.[9]

Sulfur Reduction Reaction. The sluggish SRR is one of the major intrinsic drawbacks plaguing the efficiencies of the LSBs. This also results in the extended exposure time of Li_2S_n to the electrolytes, worsening the shuttle phenomenon and inefficient sulfur utilization.[5] In addition to the improved ionic diffusivity, we elucidate how MoS_2 and MoS_2/C12A7:e^- cathode hosts contribute to accelerating the SRR during the operation of the LSBs. Figure 7a shows the ΔG profiles of the SRR of transforming S_8 to Li_2S in the presence of MoS_2 and MoS_2/C12A7:e^-, as calculated from eq 2. The first steps ΔG_1 for converting solid S_8 to liquid Li_2S_8 are the spontaneously exothermic processes ($\Delta G < 0$) on both MoS_2 and MoS_2/C12A7:e^-, releasing the energies of −3.338 and −3.325 eV, respectively. The initial transition from the S_8 ring to the long-change Li_2S_8 is an energetically favorable process as found experimentally.[9] Comparatively, the obtained values are even less than −3.016 eV for converting solid S_8 to liquid Li_2S_8 in vacuum. This means that the processes with the cathode hosts enable the release of more energy to allow Li_2S_8 to be in a more stable state than that in the vacuum. This corroborates with the occurrence of Li_2S_8 in the discharging voltage profile.[5] Likewise, the second reduction steps ΔG_2 for the Li_2S_8-to-Li_2S_6 transition on MoS_2, MoS_2/C12A7:e^-, and in vacuum remain the

https://doi.org/10.1021/acsami.4c05810
ACS Appl. Mater. Interfaces 2024, 16, 37994−38005

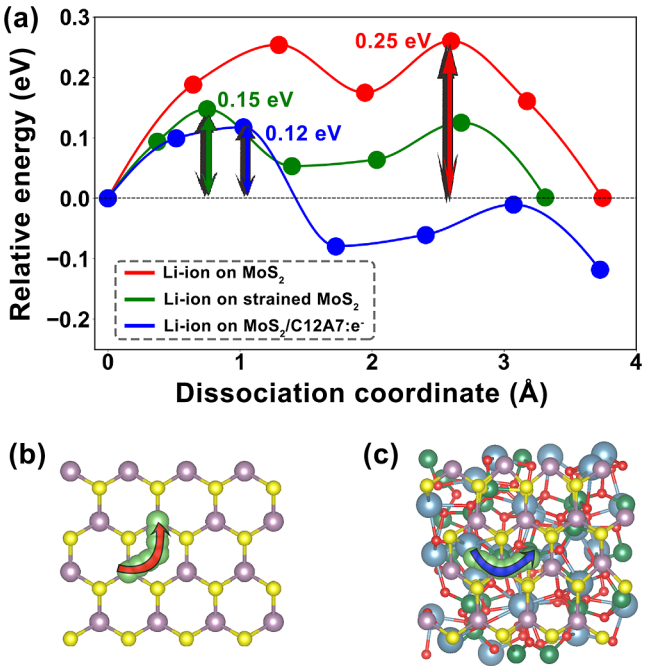

Figure 6. (a) Diffusion barriers of Li^+ ion and (b,c) corresponding path on MoS_2 and MoS_2/C12A7:e^-.

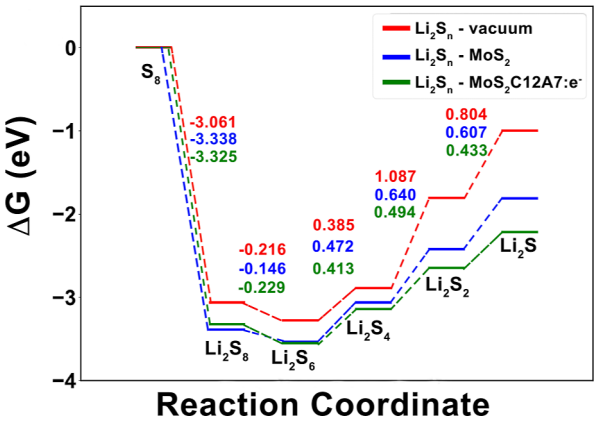

Figure 7. Gibbs free-energy profile of the sulfur reduction in a vacuum, on MoS_2, and on MoS_2/C12A7:e^-.

spontaneously exothermic processes with the significantly reduced energies of −0.146, −0.229, and −0.216 eV, respectively. This indicates the catalytic contribution of MoS_2/C12A7:e^- in accelerating the activity toward Li_2S_6.[67] On the other hand, the remaining processes including ΔG_3 (Li_2S_6-to-Li_2S_4), ΔG_4 (Li_2S_4-to-Li_2S_2), and ΔG_5 (Li_2S_2-to-Li_2S) are all endothermic. Among all discharge states, the conversion from Li_2S_4 to Li_2S_2 notably serves as the rate-determining step requiring 0.640[68] and 0.494 eV on MoS_2 and MoS_2/C12A7:e^-, respectively. This manifests that the MoS_2/C12A7:e^- hybrid plays a superior role in SRR than does MoS_2 alone. According to eq 10, the obtained rate-limiting step is predominantly ascribed to the increase in the binding energy and entropy from Li_2S_4 to Li_2S_2. Additionally, this elusive Li_2S_4-to-Li_2S_2 transition is typical in the SRR of LSBs and it is confirmed by various independent experimental studies (see the review[5]). For the sake of comparison, this value is among the lowest with other 2D cathode hosts in LSBs, such as 0.513 eV of boron nitride[69] and nitrogen-doped graphene 0.72 eV.[70] Overall, it is conclusive that MoS_2/C12A7:e^- as the cathode host can enhance the electrical transport of the cathode, suppress the shuttle effect, and offer efficient electrochemical kinetics.

CONCLUSIONS

In conclusion, we carried out first-principles DFT simulations to investigate the key aspects including electronic properties, interfacial binding, Li^+ diffusion, charge transfer mechanism, and SRR of LSBs by using MoS_2/C12A7:e^- as a cathode host. The findings indicate that the MoS_2/C12A7:e^- hybrid boosts battery efficiency over MoS_2. MoS_2 in the hybrid undergoes a semiconductor-to-metal transition, induced by electron donation from lower work function C12A7:e^-. Moreover, the resultant band positions of MoS_2/C12A7:e^- are well matched with those of the current collecting materials (*i.e.*, Cu and Ni). The hybrid cathode host effectively prevents polysulfide shuttling by forming stronger bonds with Li_2S_n than with electrolytes with Li_2S_n. This is because of charge-transfer ionic Li−S bonds. Importantly, MoS_2/C12A7:e^- not only promotes rapid reaction kinetics by reducing energy barriers for the Li^+ diffusion but also lowers the Gibbs free energies of the SRR for the effective S_8-to-Li_2S conversion.

ASSOCIATED CONTENT

Supporting Information

The Supporting Information is available free of charge at https://pubs.acs.org/doi/10.1021/acsami.4c05810.

Electronic density of states and band structure of C12A7:e^-, optimized structures of S_8 and Li_2S_n, binding energies of Li_2S_n on various 2D materials, and diffusion barriers of Li^+ on various 2D materials (PDF)

AUTHOR INFORMATION

Corresponding Author

Thanayut Kaewmaraya − *Department of Physics, Khon Kaen University, Khon Kaen 40002, Thailand; Institute of Nanomaterials Research and Innovation for Energy (IN-RIE), NANOTEC-KKU RNN on Nanomaterials Research and Innovation for Energy, Khon Kaen University, Khon Kaen 40002, Thailand;* orcid.org/0000-0002-0139-1571; Email: thakaew@kku.ac.th

Authors

Niphat Thatsami − *Department of Physics, Khon Kaen University, Khon Kaen 40002, Thailand; Institute of Nanomaterials Research and Innovation for Energy (IN-RIE), NANOTEC-KKU RNN on Nanomaterials Research and Innovation for Energy, Khon Kaen University, Khon Kaen 40002, Thailand;* orcid.org/0000-0002-9978-9288

Parinya Tangpakonsab − *Department of Physics, Khon Kaen University, Khon Kaen 40002, Thailand; Institute of Nanomaterials Research and Innovation for Energy (IN-RIE), NANOTEC-KKU RNN on Nanomaterials Research and Innovation for Energy, Khon Kaen University, Khon Kaen 40002, Thailand;* orcid.org/0000-0003-3739-4587

Pornsawan Sikam − *Office of Research Administration, Chiang Mai University, Chiang Mai 50200, Thailand; Center of Excellence in Materials Science and Technology, Materials Science Research Center, Faculty of Science, Chiang Mai University, Chiang Mai 50200, Thailand*

https://doi.org/10.1021/acsami.4c05810
ACS Appl. Mater. Interfaces 2024, 16, 37994−38005

Tanveer Hussain − *School of School of Science and Technology, University of New England, Armidale, New South Wales 2351, Australia;* orcid.org/0000-0002-0300-0503

Orapa Tamwattana − *Department of Physics, Khon Kaen University, Khon Kaen 40002, Thailand; Institute of Nanomaterials Research and Innovation for Energy (IN-RIE), NANOTEC-KKU RNN on Nanomaterials Research and Innovation for Energy, Khon Kaen University, Khon Kaen 40002, Thailand*

Anucha Watcharapasorn − *Center of Excellence in Materials Science and Technology, Materials Science Research Center, Faculty of Science, Department of Physics and Materials Science, Faculty of Science, and Center of Excellence in Quantum Technology, Faculty of Engineering, Chiang Mai University, Chiang Mai 50200, Thailand*

Pairot Moontragoon − *Department of Physics, Khon Kaen University, Khon Kaen 40002, Thailand; Institute of Nanomaterials Research and Innovation for Energy (IN-RIE), NANOTEC-KKU RNN on Nanomaterials Research and Innovation for Energy, Khon Kaen University, Khon Kaen 40002, Thailand*

Biswarup Pathak − *Department of Chemistry, Indian Institute of Technology Indore, Indore 453552, India;* orcid.org/0000-0002-9972-9947

Complete contact information is available at: https://pubs.acs.org/10.1021/acsami.4c05810

Notes

The authors declare no competing financial interest.

■ ACKNOWLEDGMENTS

This work is financially supported by the Office of the Ministry of Higher Education, Science, Research and Innovation, Thailand (grant no. RGNS63-005). T.K. acknowledges the high-performance computing facility provided by ThaiSC. Furthermore, T.K. would like to acknowledge Prof. Vittaya Amornkitbamrung for his kind mentoring. This work was supported by the NCI Adapter Scheme, with computational resources provided by NCI Australia, an NCRIS-enabled capability supported by the Australian Government. A.W. and P.S. would like to acknowledge funding support from the NSRF via the Program Management Unit for Human Resources and Institutional Development, Research and Innovation (grant nos. B05F640218 and B05F650023), National Higher Education Science Research and Innovation Policy Council, and Chiang Mai University.

■ REFERENCES

(1) Ye, H.; Li, Y. Room-Temperature Metal−Sulfur Batteries: What Can We Learn from Lithium−Sulfur? *InfoMat* **2022**, *4*, No. e12291.

(2) Yang, C.; Chen, J.; Ji, X.; Pollard, T. P.; Lü, X.; Sun, C. J.; Hou, S.; Liu, Q.; Liu, C.; Qing, T.; Wang, Y.; Borodin, O.; Ren, Y.; Xu, K.; Wang, C. Aqueous Li-Ion Battery Enabled by Halogen Conversion−Intercalation Chemistry in Graphite. *Nature* **2019**, *569* (7755), 245−250.

(3) Sun, J.; Kang, F.; Yan, D.; Ding, T.; Wang, Y.; Zhou, X.; Zhang, Q. Recent Progress in Using Covalent Organic Frameworks to Stabilize Metal Anodes for Highly-Efficient Rechargeable Batteries. *Angew. Chem., Int. Ed.* **2024**, *63*, No. e202406511.

(4) Manthiram, A.; Fu, Y.; Su, Y. S. Challenges and Prospects of Lithium-Sulfur Batteries. *Acc. Chem. Res.* **2013**, *46* (5), 1125−1134.

(5) Shao, Q.; Zhu, S.; Chen, J. A Review on Lithium-Sulfur Batteries: Challenge, Development, and Perspective. *Nano Res.* **2023**, *16*, 8097−8138.

(6) Zhao, M.; Li, B. Q.; Zhang, X. Q.; Huang, J. Q.; Zhang, Q. A Perspective toward Practical Lithium-Sulfur Batteries. *ACS Cent. Sci.* **2020**, *6* (7), 1095−1104.

(7) Qu, Z.; Zhang, X.; Xiao, R.; Sun, Z.; Li, F. Application of Organosulfur Compounds in Lithium-Sulfur Batteries. *Acta Phys. Chim. Sin.* **2023**, *0*, 2301019.

(8) Zhou, W.; Guo, B.; Gao, H.; Goodenough, J. B. Low-Cost Higher Loading of a Sulfur Cathode. *Adv. Energy Mater.* **2016**, *6* (5), 1502059.

(9) Peng, L.; Wei, Z.; Wan, C.; Li, J.; Chen, Z.; Zhu, D.; Baumann, D.; Liu, H.; Allen, C. S.; Xu, X.; Kirkland, A. I.; Shakir, I.; Almutairi, Z.; Tolbert, S.; Dunn, B.; Huang, Y.; Sautet, P.; Duan, X. A Fundamental Look at Electrocatalytic Sulfur Reduction Reaction. *Nat. Catal.* **2020**, *3* (9), 762−770.

(10) Wang, Y.; Zhou, D.; Palomares, V.; Shanmukaraj, D.; Sun, B.; Tang, X.; Wang, C.; Armand, M.; Rojo, T.; Wang, G. Revitalising Sodium-Sulfur Batteries for Non-High-Temperature Operation: A Crucial Review. *Energy Environ. Sci.* **2020**, *13*, 3848−3879.

(11) Mikhaylik, Y. V.; Akridge, J. R. Polysulfide Shuttle Study in the Li/S Battery System. *J. Electrochem. Soc.* **2004**, *151* (11), A1969.

(12) Zhou, L.; Danilov, D. L.; Eichel, R. A.; Notten, P. H. L. Host Materials Anchoring Polysulfides in Li−S Batteries Reviewed. *Adv. Energy Mater.* **2021**, *11*, 2001304.

(13) Peng, H. J.; Zhang, Q. Designing Host Materials for Sulfur Cathodes: From Physical Confinement to Surface Chemistry. *Angew. Chem., Int. Ed.* **2015**, *54* (38), 11018−11020.

(14) Ma, Q.; Zheng, Y.; Luo, D.; Or, T.; Liu, Y.; Yang, L.; Dou, H.; Liang, J.; Nie, Y.; Wang, X.; Yu, A.; Chen, Z. 2D Materials for All-Solid-State Lithium Batteries. *Adv. Mater.* **2022**, *34*, 2108079.

(15) Sun, Z.; Zhang, J.; Yin, L.; Hu, G.; Fang, R.; Cheng, H. M.; Li, F. Conductive Porous Vanadium Nitride/Graphene Composite as Chemical Anchor of Polysulfides for Lithium-Sulfur Batteries. *Nat. Commun.* **2017**, *8*, 14627.

(16) Zhang, Q.; Zhang, X.; Xiao, Y.; Li, C.; Tan, H. H.; Liu, J.; Wu, Y. Theoretical Insights into the Favorable Functionalized Ti_2C-Based MXenes for Lithium-Sulfur Batteries. *ACS Omega* **2020**, *5* (45), 29272−29283.

(17) Al-Jayyousi, H. K.; Sajjad, M.; Liao, K.; Singh, N. Two-Dimensional Biphenylene: A Promising Anchoring Material for Lithium-Sulfur Batteries. *Sci. Rep.* **2022**, *12* (1), 4653.

(18) Sun, W.; Song, Z.; Feng, Z.; Huang, Y.; Xu, Z. J.; Lu, Y. C.; Zou, Q. Carbon-Nitride-Based Materials for Advanced Lithium−Sulfur Batteries. *Nano-Micro Lett.* **2022**, *14*, 222.

(19) Panigrahi, P.; Pal, Y.; Hussain, T.; Ahuja, R. Application of Germanene Monolayers as Efficient Anchoring Material to Immobilize Lithium Polysulfides in Li-S Batteries. *Appl. Surf. Sci.* **2021**, *558*, 149850.

(20) Singh, D.; Gupta, S. K.; Hussain, T.; Sonvane, Y.; Gajjar, P. N.; Ahuja, R. Antimonene Allotropes α- and β-Phases as Promising Anchoring Materials for Lithium−Sulfur Batteries. *Energy Fuels* **2021**, *35* (10), 9001−9009.

(21) Mahankali, K.; Thangavel, N. K.; Gopchenko, D.; Arava, L. M. R. Atomically Engineered Transition Metal Dichalcogenides for Liquid Polysulfide Adsorption and Their Effective Conversion in Li-S Batteries. *ACS Appl. Mater. Interfaces* **2020**, *12* (24), 27112−27121.

(22) Luo, P.; Zhuge, F.; Zhang, Q.; Chen, Y.; Lv, L.; Huang, Y.; Li, H.; Zhai, T. Doping Engineering and Functionalization of Two-Dimensional Metal Chalcogenides. *Nanoscale Horiz.* **2019**, *4*, 26−51.

(23) Nicolosi, V.; Chhowalla, M.; Kanatzidis, M. G.; Strano, M. S.; Coleman, J. N. Liquid Exfoliation of Layered Materials. *Science* **2013**, *340*, 1226419.

(24) Liu, F.; Wang, N.; Shi, C.; Sha, J.; Ma, L.; Liu, E.; Zhao, N. Phosphorus Doping of 3D Structural MoS_2 to Promote Catalytic Activity for Lithium-Sulfur Batteries. *Chem. Eng. J.* **2022**, *431*, 133923.

(25) Zhang, B. W.; Cao, L.; Tang, C.; Tan, C.; Cheng, N.; Lai, W. H.; Wang, Y. X.; Cheng, Z. X.; Dong, J.; Kong, Y.; Dou, S. X.; Zhao, S. Atomically Dispersed Dual-Site Cathode with a Record High Sulfur Mass Loading for High-Performance Room-Temperature Sodium−Sulfur Batteries. *Adv. Mater.* **2023**, *35* (1), 2206828.

(26) Wang, Y.; Lai, Y.; Chu, J.; Yan, Z.; Wang, Y. X.; Chou, S. L.; Liu, H. K.; Dou, S. X.; Ai, X.; Yang, H.; Cao, Y. Tunable Electrocatalytic Behavior of Sodiated MoS_2 Active Sites toward Efficient Sulfur Redox Reactions in Room-Temperature Na−S Batteries. *Adv. Mater.* **2021**, *33* (16), 2100229.
(27) Wang, S.; Feng, S.; Liang, J.; Su, Q.; Zhao, F.; Song, H.; Zheng, M.; Sun, Q.; Song, Z.; Jia, X.; Yang, J.; Li, Y.; Liao, J.; Li, R.; Sun, X. Insight into MoS_2−MoN Heterostructure to Accelerate Polysulfide Conversion toward High-Energy-Density Lithium−Sulfur Batteries. *Adv. Energy Mater.* **2021**, *11* (11), 2003314.
(28) Kim, S.; Song, S.; Park, J.; Yu, H. S.; Cho, S.; Kim, D.; Baik, J.; Choe, D. H.; Chang, K. J.; Lee, Y. H.; Kim, S. W.; Yang, H. Long-Range Lattice Engineering of $MoTe_2$ by a 2D Electride. *Nano Lett.* **2017**, *17* (6), 3363−3368.
(29) Hosono, H.; Kitano, M. Advances in Materials and Applications of Inorganic Electrides. *Chem. Rev.* **2021**, *121* (5), 3121−3185.
(30) Dye, J. L. Electrides: Ionic Salts with Electrons as the Anions. *Science* **1990**, *247* (4943), 663−668.
(31) Matsuishi, S.; Toda, Y.; Miyakawa, M.; Hayashi, K.; Kamiya, T.; Hirano, M.; Tanaka, I.; Hosono, H. High-Density Electron Anions in a Nanoporous Single Crystal: $[Ca_{24}Al_{28}O_{64}]^{4+}$ $(4e^-)$. *Science* **2003**, *301* (5633), 626−629.
(32) Tangpakonsab, P.; Banlusan, K.; Moontragoon, P.; Namuangruk, S.; Amornkitbamrung, V.; Kaewmaraya, T. Electronic Structures and Optical Properties of Nanoporous Complex Oxide $12CaO{\cdot}7Al_2O_3$ (C12A7) under High Pressure. *Comput. Mater. Sci.* **2021**, *194*, 110456.
(33) Feizi, E.; Ray, A. K. $12CaO{\cdot}7Al_2O_3$ Ceramic: A Review of the Electronic and Optoelectronic Applications in Display Devices. *J. Display Technol.* **2016**, *12* (5), 451−459.
(34) Hara, M.; Kitano, M.; Hosono, H. Ru-Loaded C12A7:e^- Electride as a Catalyst for Ammonia Synthesis. *ACS Catal.* **2017**, *7* (4), 2313−2324.
(35) Hosono, H.; Kim, J.; Toda, Y.; Kamiya, T.; Watanabe, S. Transparent Amorphous Oxide Semiconductors for Organic Electronics: Application to Inverted OLEDs. *Proc. Natl. Acad. Sci. U.S.A.* **2017**, *114* (2), 233−238.
(36) Toda, Y.; Hirayama, H.; Kuganathan, N.; Torrisi, A.; Sushko, P. V.; Hosono, H. Activation and Splitting of Carbon Dioxide on the Surface of an Inorganic Electride Material. *Nat. Commun.* **2013**, *4*, 2378.
(37) Kresse, G.; Furthmüller, J. Efficient Iterative Schemes for Ab Initio Total-Energy Calculations Using a Plane-Wave Basis Set. *Phys. Rev. B: Condens Matter Mater. Phys.* **1996**, *54* (16), 11169−11186.
(38) Kresse, G.; Furthmüller, J. Efficiency of Ab-Initio Total Energy Calculations for Metals and Semiconductors Using a Plane-Wave Basis Set. *Comput. Mater. Sci.* **1996**, *6* (1), 15−50.
(39) Perdew, J. P.; Burke, K.; Ernzerhof, M. Generalized Gradient Approximation Made Simple. *Phys. Rev. Lett.* **1996**, *77* (18), 3865−3868.
(40) Blöchl, P. E. Projector Augmented-Wave Method. *Phys. Rev. B* **1994**, *50* (24), 17953−17979.
(41) Monkhorst, H. J.; Pack, J. D. Special Points for Brillouin-Zone Integrations. *Phys. Rev. B* **1976**, *13* (12), 5188−5192.
(42) Grimme, S.; Antony, J.; Ehrlich, S.; Krieg, H. A Consistent and Accurate Ab Initio Parametrization of Density Functional Dispersion Correction (DFT-D) for the 94 Elements H-Pu. *J. Chem. Phys.* **2010**, *132* (15), 154104.
(43) Henkelman, G.; Jónsson, H. Improved Tangent Estimate in the Nudged Elastic Band Method for Finding Minimum Energy Paths and Saddle Points. *J. Chem. Phys.* **2000**, *113* (22), 9978−9985.
(44) Deringer, V. L.; Tchougréeff, A. L.; Dronskowski, R. Crystal Orbital Hamilton Population (COHP) Analysis as Projected from Plane-Wave Basis Sets. *J. Phys. Chem. A* **2011**, *115* (21), 5461−5466.
(45) Aubert, E.; Lebègue, S.; Marsman, M.; Bui, T. T. T.; Jelsch, C.; Dahaoui, S.; Espinosa, E.; Ángyán, J. G. Periodic Projector Augmented Wave Density Functional Calculations on the Hexachlorobenzene Crystal and Comparison with the Experimental Multipolar Charge Density Model. *J. Phys. Chem. A* **2011**, *115* (50), 14484−14494.
(46) Liu, R.; Wei, Z.; Peng, L.; Zhang, L.; Zohar, A.; Schoeppner, R.; Wang, P.; Wan, C.; Zhu, D.; Liu, H.; Wang, Z.; Tolbert, S. H.; Dunn, B.; Huang, Y.; Sautet, P.; Duan, X. Establishing Reaction Networks in the 16-Electron Sulfur Reduction Reaction. *Nature* **2024**, *626* (7997), 98−104.
(47) Wang, Z. M., Ed.; *MoS_2 Materials, Physics, and Devices*; Springer International Publishing: Cham, 2014; Vol. *21*.
(48) Fang, Q.; Li, M.; Zhao, X.; Yuan, L.; Wang, B.; Xia, C.; Ma, F. Van Der Waals Graphene/MoS_2 heterostructures: Tuning the Electronic Properties and Schottky Barrier by Applying a Biaxial Strain. *Mater. Adv.* **2022**, *3* (1), 624−631.
(49) Radisavljevic, B.; Radenovic, A.; Brivio, J.; Giacometti, V.; Kis, A. Single-Layer MoS2 Transistors. *Nat. Nanotechnol.* **2011**, *6* (3), 147−150.
(50) Sushko, P. V.; Shluger, A. L.; Hirano, M.; Hosono, H. From Insulator to Electride: A Theoretical Model of Nanoporous Oxide $12CaO{\cdot}7Al_2O_3$. *J. Am. Chem. Soc.* **2007**, *129* (4), 942−951.
(51) Shannon, R. D. Revised Effective Ionic Radii and Systematic Studies of Interatomic Distances in Halides and Chalcogenides. *Acta Crystallogr., Sect. A* **1976**, *32* (5), 751−767.
(52) Shaukat, A.; Saeed, Y.; Ikram, N.; Akbarzadeh, H. First Principles Calculations of Structural, Electronic and Optical Properties of Various Phases of CaS. *Eur. Phys. J. B* **2008**, *62* (4), 439−446.
(53) Mullay, J. Estimation of Atomic and Group Electronegativities; *Electronegativity Structure and Bonding*; Sen, K. D., Jørgensen, C. K., Eds.; Springer. 2005, 1−25.
(54) Michaelson, H. B. The Work Function of the Elements and Its Periodicity. *J. Appl. Phys.* **1977**, *48* (11), 4729−4733.
(55) Hussain, T.; Kaewmaraya, T.; Hu, Z.; Zhao, X. S. Efficient Control of the Shuttle Effect in Sodium-Sulfur Batteries with Functionalized Nanoporous Graphenes. *ACS Appl. Nano Mater.* **2022**, *5*, 12637−12645.
(56) Haseeb, H. H.; Li, Y.; Ayub, S.; Fang, Q.; Yu, L.; Xu, K.; Ma, F. Defective Phosphorene as a Promising Anchoring Material for Lithium-Sulfur Batteries. *J. Phys. Chem. C* **2020**, *124* (5), 2739−2746.
(57) Huang, X. L.; Hussain, T.; Liu, H.; Kaewmaraya, T.; Xu, M.; Liu, H. K.; Dou, S. X.; Wang, Z. Dredging Sodium Polysulfides Using a Fe_3C Electrocatalyst to Realize Improved Room-Temperature Na-S Batteries. *Inorg. Chem. Front.* **2023**, *10* (14), 4241−4251.
(58) Nahian, M. S.; Jayan, R.; Islam, M. M. Atomic-Scale Insights into Comparative Mechanisms and Kinetics of Na-S and Li-S Batteries. *ACS Catal.* **2022**, *12*, 7664−7676.
(59) Kaewmaraya, T.; Thatsami, N.; Tangpakonsab, P.; Klinkla, R.; Kotmool, K.; Hussian, T. Revealing the Binding Mechanism of Redox Intermediates in Sodium−Sulfur Batteries by Two-Dimensional Janus Monolayers. *J. Power Sources* **2023**, *585*, 233639.
(60) Zhou, G.; Tian, H.; Jin, Y.; Tao, X.; Liu, B.; Zhang, R.; Seh, Z. W.; Zhuo, D.; Liu, Y.; Sun, J.; Zhao, J.; Zu, C.; Wu, D. S.; Zhang, Q.; Cui, Y. Catalytic Oxidation of Li_2S on the Surface of Metal Sulfides for Li-S Batteries. *Proc. Natl. Acad. Sci. U.S.A.* **2017**, *114* (5), 840−845.
(61) Laidler, K. J. The Development of the Arrhenius Equation. *J. Chem. Educ.* **1984**, *61* (6), 494.
(62) Tao, X.; Wan, J.; Liu, C.; Wang, H.; Yao, H.; Zheng, G.; Seh, Z. W.; Cai, Q.; Li, W.; Zhou, G.; Zu, C.; Cui, Y. Balancing Surface Adsorption and Diffusion of Lithium-Polysulfides on Nonconductive Oxides for Lithium-Sulfur Battery Design. *Nat. Commun.* **2016**, *7*, 11203.
(63) Sun, X.; Wang, Z.; Fu, Y. Q. Defect-Mediated Lithium Adsorption and Diffusion on Monolayer Molybdenum Disulfide. *Sci. Rep.* **2015**, *5*, 18712.
(64) Zheng, J.; Ren, Z.; Guo, P.; Fang, L.; Fan, J. Diffusion of Li^+ Ion on Graphene: A DFT Study. *Appl. Surf. Sci.* **2011**, *258* (5), 1651−1655.
(65) Zhou, G.; Zhao, S.; Wang, T.; Yang, S. Z.; Johannessen, B.; Chen, H.; Liu, C.; Ye, Y.; Wu, Y.; Peng, Y.; Liu, C.; Jiang, S. P.; Zhang, Q.; Cui, Y. Theoretical Calculation Guided Design of Single-Atom Catalysts toward Fast Kinetic and Long-Life Li-S Batteries. *Nano Lett.* **2020**, *20* (2), 1252−1261.
(66) Hammer, B.; Norskov, J. K. Why Gold Is the Noblest of All the Metals. *Nature* **1995**, *376* (6537), 238−240.
(67) Lin, H.; Yang, L.; Jiang, X.; Li, G.; Zhang, T.; Yao, Q.; Zheng, G. W.; Lee, J. Y. Electrocatalysis of Polysulfide Conversion by Sulfur-

https://doi.org/10.1021/acsami.4c05810
ACS Appl. Mater. Interfaces 2024, 16, 37994−38005

Deficient MoS_2 Nanoflakes for Lithium-Sulfur Batteries. *Energy Environ. Sci.* **2017**, *10* (6), 1476−1486.
(68) Shao, Q.; Lu, P.; Xu, L.; Guo, D.; Gao, J.; Wu, Z. S.; Chen, J. Rational Design of MoS_2 Nanosheets Decorated on Mesoporous Hollow Carbon Spheres as a Dual-Functional Accelerator in Sulfur Cathode for Advanced Pouch-Type Li−S Batteries. *J. Energy Chem.* **2020**, *51*, 262−271.
(69) Khossossi, N.; Singh, D.; Essaoudi, I.; Ahuja, R.; Ainane, A. Unveiling the Catalytic Potential of Two-Dimensional Boron Nitride in Lithium−Sulfur Batteries. *Chem. Eng. J.* **2024**, *479*, 147518.
(70) Du, Z.; Chen, X.; Hu, W.; Chuang, C.; Xie, S.; Hu, A.; Yan, W.; Kong, X.; Wu, X.; Ji, H.; Wan, L. J. Cobalt in Nitrogen-Doped Graphene as Single-Atom Catalyst for High-Sulfur Content Lithium-Sulfur Batteries. *J. Am. Chem. Soc.* **2019**, *141* (9), 3977−3985.

https://doi.org/10.1021/acsami.4c05810
ACS Appl. Mater. Interfaces 2024, 16, 37994−38005